Journal of Alloys and Compounds 480 (2009) 340–346

Contents lists available at ScienceDirect

Journal of Alloys and Compounds

journal homepage: www.elsevier.com/locate/jallcom

Microstructural modification and mechanical property improvement in friction stir zone of thixo-molded AE42 Mg alloy

Lina Yu[a,*], Kazuhiro Nakata[a], Jinsun Liao[b]

[a] Joining and Welding Research Institute, Osaka University, Osaka, Japan
[b] Kurimoto, Ltd., Osaka, Japan

ARTICLE INFO

Article history:
Received 27 January 2009
Received in revised form 3 February 2009
Accepted 3 February 2009
Available online 20 February 2009

Keywords:
Microstructure
Mechanical property
FSW
AE42 Mg alloy
Thixo-molded

ABSTRACT

Thixo-molded AE42 Mg alloy was friction stir welded, and the soundness of joints was evaluated, together with the microstructure evolution and mechanical properties in friction stir zones. According to X-ray radiography, the optimum FSW condition range of AE42 alloy exists between AZ61 and AZ31 alloys, and it seems that the optimum welding condition range increases with decreasing Al content in the Mg alloys. There are mainly two kinds of compounds in the thixo-molded AE42 alloy, and FSW has little influence on the grainy $Al_{10}RE_2Mn_7$ compound, but it has great influence on $Al_{11}RE_3$ phase, which is changed from lamellar eutectic to small particles after welding. Furthermore, the average diameter of $Al_{11}RE_3$ particles in SZ decreases with increasing the traveling speed at constant rotation speed due to less heat input. The hardness in SZ is higher than that in BM, and tensile strength and elongation are both improved after welding because the stirring refines and uniforms the microstructure and intermetallic compounds.

1. Introduction

Under consideration of fuel economy in automotive and aerospace industries, Mg alloys have been adopted and are expected to be extensively used in the future, due to their excellent specific mechanical properties, such as high strength to weight ratios, and lightweight [1–3]. With their increasing demand of industrial application, it is necessary to develop effective welding techniques for the joining of Mg alloys. However, fusion welding of these materials is difficult due to the formation of vast porosity. Friction stir welding (FSW), a novel solid joining technology, is a potential candidate because of its many advantages compared with the traditional fusion welding processes [4,5]. It can produce pore-free joints where the pores caused by casting solidification are eliminated, and fine-grained structures are generated in the stir zones where dynamic recrystallization occurs [6–9].

In previous studies, FSW of Mg alloys are mainly focused on the die-cast and extruded AZ alloys and AM alloys [10–13]. Although there is a few research works about the die-cast AE42 alloy [14], a heat-resistant alloy with superior creep resistance due to the existence of intermetallic compounds at grain boundaries, the information on its microstructural evolution and mechanical properties in the welded joints is limited. In the present work, the thixo-molded AE42 Mg alloy was friction stir welded, and the microstructure and mechanical properties after FSW were extensively investigated.

2. Experimental procedures

The material used in present study is heat resistant AE42 alloy, which was semi-solid injection cast by thixo-molding, with the chemical composition listed in Table 1. The sheet was 150 mm × 90 mm × 5 mm in specimen size, and the surface was degreased with acetone before welding. Stir-in-plate welding was performed using a load-controlled type FSW machine with the welding and tool parameters shown in Tables 2 and 3, respectively. The tool rotation speed was changed from 1000 to 1750 rpm, while the traveling speed was ranged from 150 to 1250 mm/min.

After welding, the welded joints were examined by X-ray radiography, and the metallurgical inspections were performed on the cross-section of the joints for metallographic analysis. The metallographic specimens were first mechanically polished and then etched with the solution containing 1 ml nitric acid, 75 ml ethylene glycol, and 24 ml water. The microstructures of the welded specimens were observed with the optical microscope (OM) and the scanning electron microscope (SEM). In order to examine in detail the microstructure in the stir zone, the size of intermetallic particles in stir zone was statistically determined using an image processing method (Image-Pro Plus ver.4.0).

The hardness measurement was performed on the metallographic specimens crossing the joints at mid thickness. Tensile samples of 2 mm in thickness were cut from the stir zone and base material at mid thickness with the top and bottom surfaces eliminated. Furthermore, the facture surface after the tensile test was examined by SEM.

3. Results and discussion

3.1. Optimum FSW condition range of thixo-molded AE42 alloy

According to the results of X-ray radiography, the optimum FSW condition range (without any defect) of thixo-molded AE42 alloy

* Corresponding author. Tel.: +81 6 6879 8668; fax: +81 6 6879 8668.
E-mail address: yuxueer33@hotmail.com (L. Yu).

0925-8388/$ – see front matter © 2009 Elsevier B.V. All rights reserved.
doi:10.1016/j.jallcom.2009.02.015

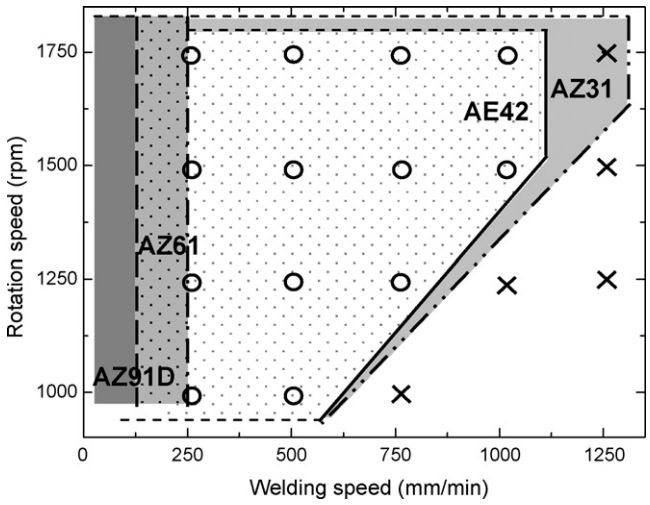

Fig. 1. Optimum FSW condition range of several kinds of Mg alloys (○,defect-free; ×,defect).

Table 1
Chemical composition of thixo-molded AE42 Mg alloy.

Alloy	Chemical compositions (mass %)						
	Al	Mn	RE	Cu	Ni	Fe	Mg
AE42	4.0	0.1	2.5	0.0015	< 0.0005	< 0.0005	Bal.

Table 2
FSW parameters.

Load	9.8 kN
Tool rotation speed	1000–1750 rpm
Traveling speed	150–1250 mm/min

is obtained, as shown in Fig. 1, together with three other kinds of Mg alloys, AZ91D, AZ61 and AZ31, reported in Ref. [15]. Apparently, the optimum condition ranges of AZ91D and AZ61 alloys are relatively narrow, indicating that they cannot be welded with too fast traveling speed, while the welding ranges of AE42 and AZ31 alloys are much wider. The optimum FSW welding range of thixo-molded AE42 alloy exists between AZ61 and AZ31 alloys. It seems that the optimum condition range is related to the Al content in Mg alloys, and the lower Al content is beneficial to FSW because the high content of Al may increase the strength of Mg alloy and result in the decrease of plastic deformability.

Table 3
Conditions of the FSW tool.

Material of tool	SKD61
Diameter of shoulder	15 mm
Diameter of probe	M5
Length of probe	4.9 mm
Taper angle of shoulder	3°

3.2. Microstructures in friction stir welded joint

Fig. 2(a) shows the overview of the cross-section of thixo-molded AE42 alloy welded with the rotation speed of 1250 rpm and the traveling speed of 250 mm/min, and the microstructures at stir zone (SZ), thermo-mechanically affected zone (TMAZ) and base metal (BM) are given in Fig. 2(b–d), respectively. The BM exhibits a typical solidification structure formed in the casting process, having a dendritic microstructure with α-Mg phase and eutectic phase. Grains in the TMAZ have been deformed greatly after stirring due to the heat effect and mechanical deformation, and the grains have obvious orientation along the metal-flow direction induced by stirring. The SZ contains a fine recrystallized structure instead of dendritic one, and the intermetallic compound (dark phase in Fig. 2) seems to be uniformly dispersed in the SZ.

With higher magnification, as shown in Fig. 3(a), a typical casting microstructure is observed in the BM of thixo-molded AE42 alloy, which is characterized by primary α-Mg dendrites and intermetallic phases at grain boundaries or in the interdendritic regions. The intermetallic phases in BM can be mainly classified into two types: one with a lamellar-like morphology and the other with a grainy shape, and the lamellar-like phase is the dominant intermetallic phase. As presented in Fig. 3(b), the lamellar-like phase has obvious orientation in TMAZ, and some of them have been fractured to smaller particles due to the mechanical deformation caused by stirring. Compared with BM, the grainy phase nearly has no change in TMAZ. In SZ as illustrated by Fig. 3(c), the edge of the grainy particle has become more smooth and slick caused by the friction in the stirring process, however, they still keep the similar morphology and size with those in BM and TMAZ. In contrast, the lamellar-like phase in SZ has remarkably been changed from lamellar eutectic to small particles after stirring. This is probably related to its instability due to the lamellar structure.

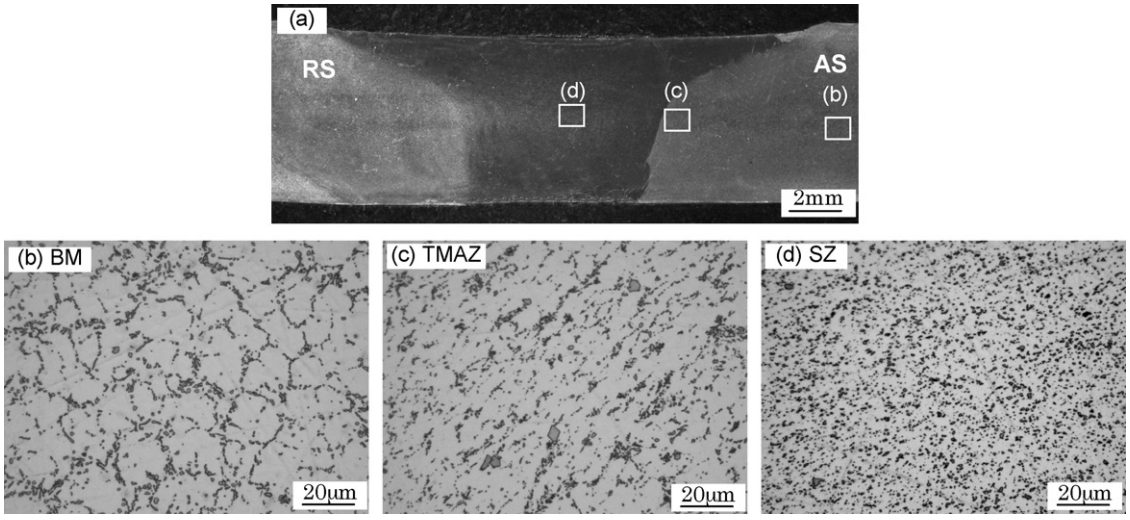

Fig. 2. Macro and microstructures of thixo-molded AE42 alloy welded with the rotation speed of 1250 rpm and the traveling speed of 250 mm/min.

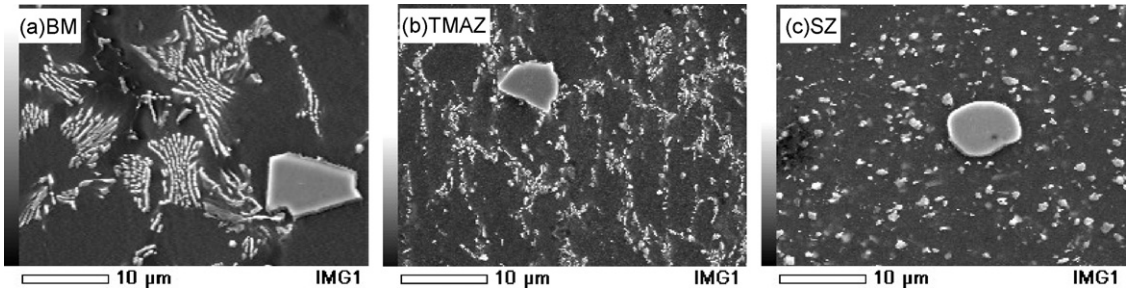

Fig. 3. Microstructures with high magnification in different positions welded with the traveling speed of 250 mm/min and the rotation speed of 1250 rpm: (a) BM; (b) TMAZ; (c) SZ.

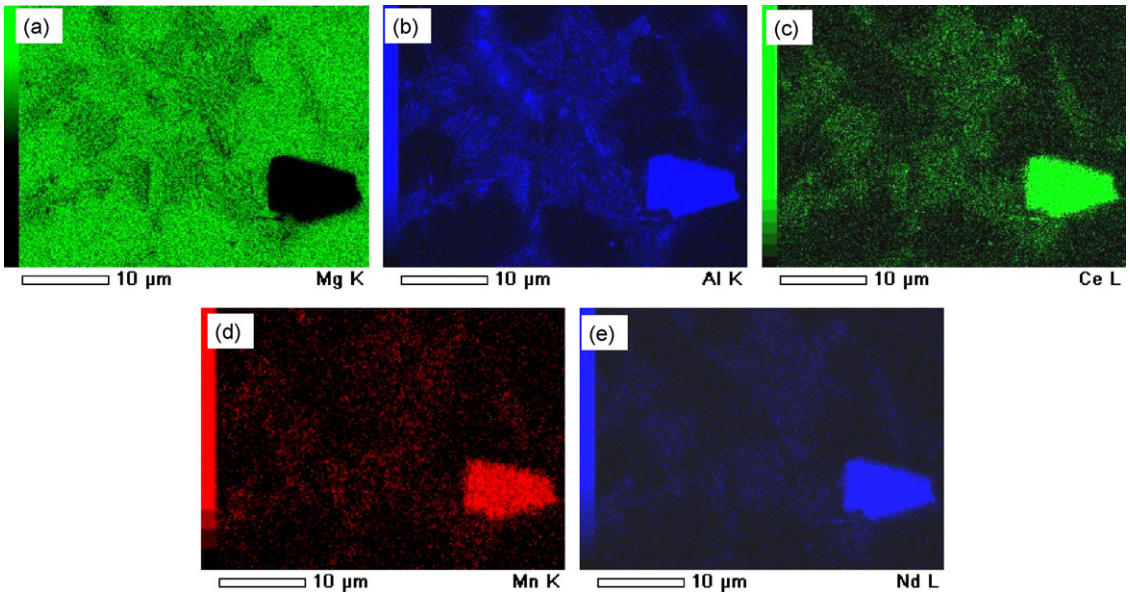

Fig. 4. SEM map analysis of the base metal of thixo-molded AE42 alloy shown in Fig. 3(a).

The two types of intermetallic phases were further analyzed by EDX to determine their compositions. The element map analysis of Fig. 3(a) is presented in Fig. 4. It shows that the dominant lamellar-like phase mainly contains Al and Ce/Nd elements, which should be $Al_{11}RE_3$ (body-centered orthorhombic, $a = 0.45$ nm, $b = 1.32$ nm and $c = 0.99$ nm), as reported in Ref. [16]. While the minor grainy shape phase contains Al, Ce, Nd and Mn elements, indicating that it may be the complex $Al_{10}RE_2Mn_7$ (hexagonal, $a = 0.90$ nm and $c = 1.30$ nm), as identified by Pettersen et al. [17]. Between the lamellar $Al_{11}Re_3$, there is α-Mg phase. This special structure is probably formed in the casting process by the eutectoid grow mode. The above microstructure observation suggests that, (1) two types of intermetallic phases exist in the thixo-molded AE42 alloy, i.e. lamellar-like $Al_{11}RE_3$ and grainy $Al_{10}RE_2Mn_7$, with the former being the dominant one, and (2) after friction stir welding, the lamellar-like $Al_{11}RE_3$ phase has been changed to the dispersed particles, while the grainy $Al_{10}RE_2Mn_7$ phase keeps its original morphology, with the edge more smooth and slick.

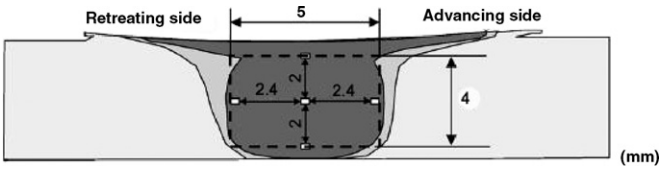

Fig. 5. Schematic illustration of the different observed positions of microstructure in SZ.

From the above analysis, it is known that mainly the $Al_{11}RE_3$ phase among the intermetallic compounds has been influenced by stirring, so the present work was focused on the $Al_{11}RE_3$ phase in SZ, and the size and distribution of $Al_{11}RE_3$ phase were investigated in detail at different positions of SZ, as shown in Figs. 5 and 6 reveals the SEM images indicating the size and distribution of $Al_{11}RE_3$ phase in (a) top, (b) retreating side (RS), (c) middle, (d) advancing side (AS), and (e) bottom of SZ in the friction stir weld with the traveling speed of 250 mm/min and the rotation speed of 1250 rpm. It is apparent that the size of $Al_{11}RE_3$ phase in the bottom position is much smaller than that in the other positions of SZ, which is considered to be caused by a higher cooling speed in the bottom position. The $Al_{11}RE_3$ particle size in the top and middle position is mostly the biggest among all the positions, and the particle size in RS is almost as same as that in AS. Furthermore, the $Al_{11}RE_3$ particles are aligned to different directions in each region, and this phenomenon is believed to be attributed to the various local metal-flow directions induced by stirring in SZ [18].

3.3. *Effect of welding parameters on the microstructure in SZ*

The microstructures in SZ welded at various traveling speeds with a constant rotation speed of 1250 rpm are shown in Fig. 7. The recrystallized structure in SZ changes with welding conditions. At the lower traveling speed of 250 mm/min, the size of the $Al_{11}RE_3$ intermetallic compound is a little bigger, and it seems to decrease with increasing the traveling speed. This result is considered to be

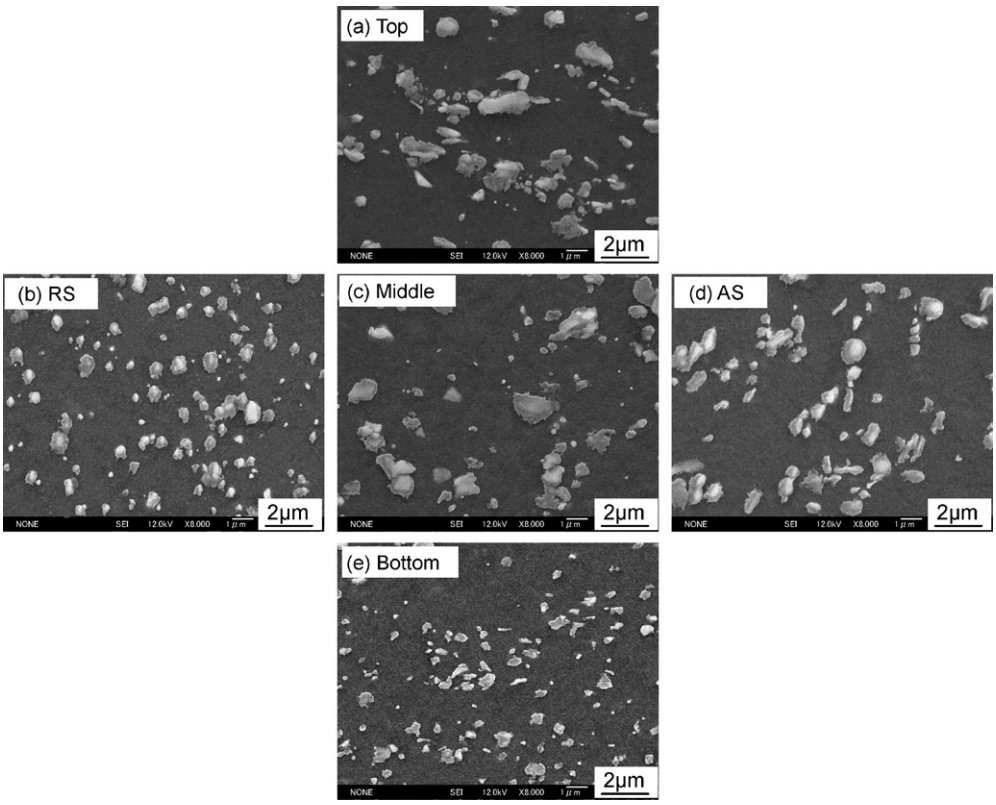

Fig. 6. SEM images of $Al_{11}RE_3$ phase in different positions of SZ welded with the traveling speed of 250 mm/min and the rotation speed of 1250 rpm: (a) top; (b) retreating side; (c) middle; (d) advancing side; (e) bottom.

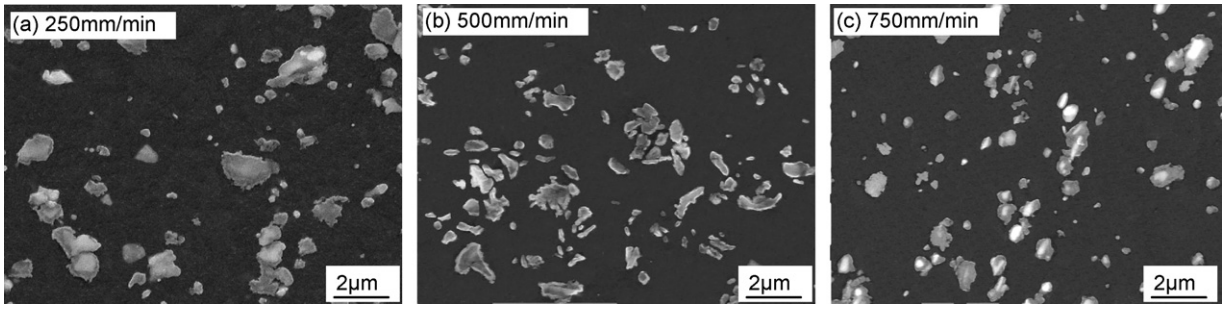

Fig. 7. Microstructures of SZ of AE42 alloys welded at various traveling speeds with a constant rotation speed of 1250 rpm.

caused by different weld heat input, and will be discussed later in detail.

Fig. 8 illustrates the relation between the average diameter of the $Al_{11}RE_3$ particle in SZ and the traveling speed at the constant rotation speed of 1250 rpm. The average diameter is calculated from the data in the five different regions of SZ as shown in Fig. 6. It is found that the average diameter of $Al_{11}RE_3$ particle in SZ remarkably decreased with increasing the traveling speed from 250 to 750 mm/min. It is because that there is no enough heat input for the intermetallic compound to grow up in the recrystallized process.

3.4. Mechanism of $Al_{11}RE_3$ phase change in SZ

As described previously, the lamellar-like $Al_{11}RE_3$ phase has been greatly changed after friction stir welding. Fig. 9 shows the SEM images of the $Al_{11}RE_3$ phase in different zones at mid-thickness of sample, which was welded with the traveling speed of 250 mm/min and the rotation speed of 1250 rpm. Some of the lamellar eutectic $Al_{11}RE_3$ phase in BM (Fig. 9(a)) have been fractured

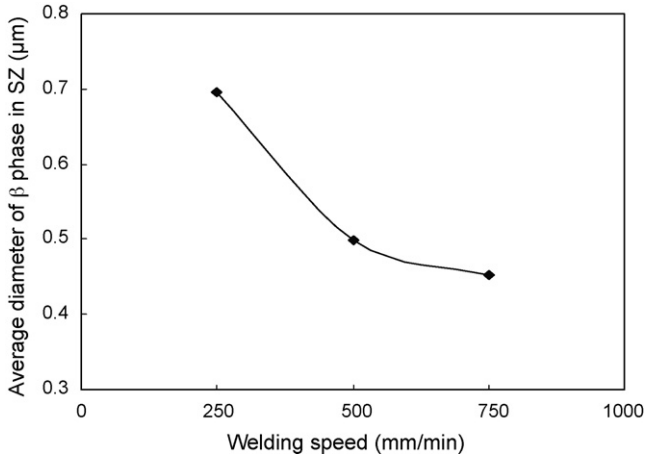

Fig. 8. Relation between average diameter of $Al_{11}RE_3$ phase in SZ and traveling speed at the constant rotation speed of 1250 rpm.

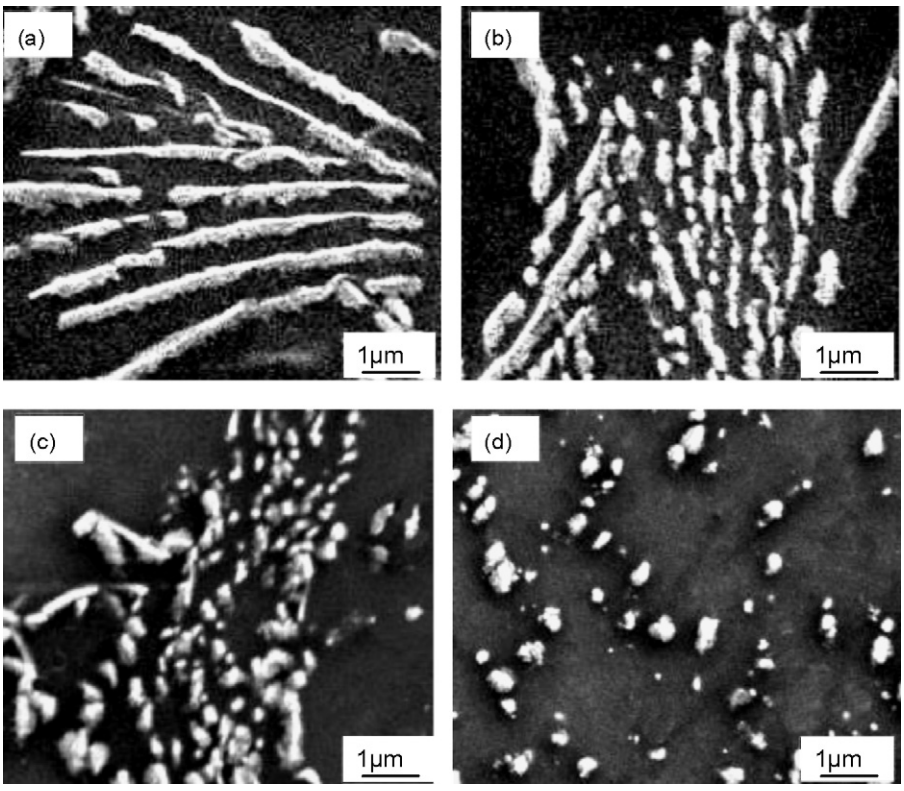

Fig. 9. SEM images of the $Al_{11}RE_3$ phase in deferent zones at mid-thickness of sample welded with traveling speed of 250 mm/min and the rotation speed of 1250 rpm: (a) BM; (b) TMAZ near BM side; (c) TMAZ near SZ side; (d) SZ.

in TMAZ near BM side (Fig. 9(b)). In TMAZ near SZ side, most $Al_{11}RE_3$ phase has been changed to particles from lamellar structure, but they are aligned along the deformed grain boundaries (Fig. 9(c)). In SZ, all the $Al_{11}RE_3$ phase is in the form of particles, which are relatively uniformly dispersed in the matrix (Fig. 9(d)).

The morphology change of $Al_{11}RE_3$ phase in various zones indicates that the $Al_{11}RE_3$ phase is just fractured from lamellar to particle from BM to TMAZ by the mechanical deformation during the stirring process. However the average diameter of $Al_{11}RE_3$ phase in SZ becomes a little bigger than that in the other positions, indicating that it has also grown up after friction stir welding. The coarsening of $Al_{11}RE_3$ phase is believed to be resulted from the heat introduced by friction stirring, and has a relation with the heat input Q. That is to say, two steps are included in the changing process of $Al_{11}RE_3$ phase, i.e. fracturing and growing-up, which are caused by the mechanical deformation and heat input, respectively.

Heat input introduced by FSW is quite important to the microstructure and the mechanical properties in SZ. Frigaard et al. [19] have suggested the following equation describing the heat input during the FSW:

$$Q = \frac{3}{4}\pi^2 \mu PNR^3 \quad (1)$$

where Q is the heat input, μ is the friction coefficient, P is the pressure, N is the rotation speed and R is the radius of the shoulder. From Eq. (1), if the heat input per unit length, Q, is considered for

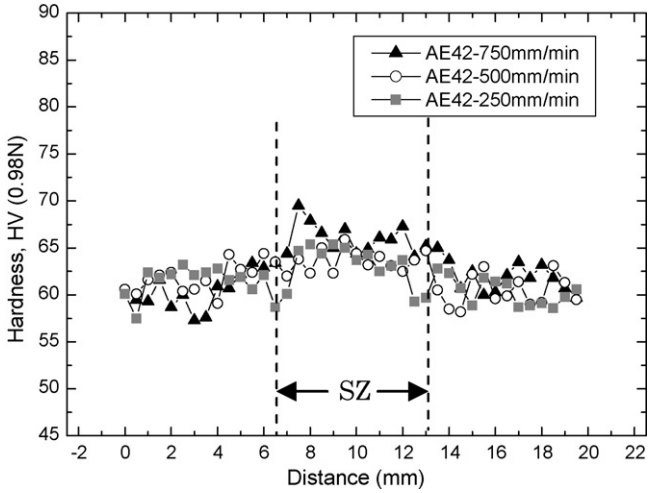

Fig. 10. Hardness of the cross-section of AE42 alloys welded at various traveling speeds with the constant rotation speed of 1250 rpm.

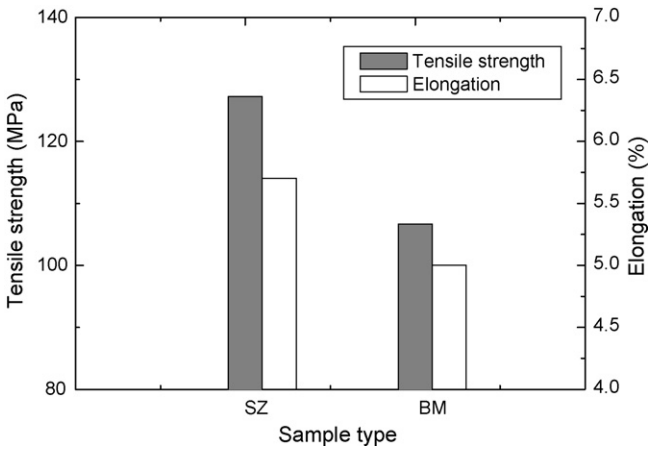

Fig. 11. Tensile strength and elongation of BM and SZ samples welded with 1250 rpm rotation speed and 250 mm/min traveling speed.

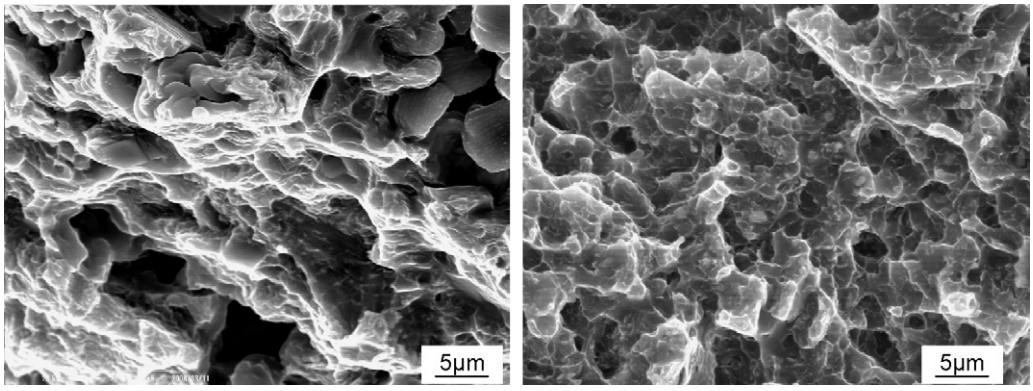

Fig. 12. Fracture surface of tensile samples: (a) BM; (b) SZ.

the moving welding, Kim et al. [20] obtained Eq. (2):

$$Q = \frac{\alpha q}{V} = \frac{4}{3}\pi^2 \frac{\alpha \mu PNR^3}{V} \quad (2)$$

where α is the heat input efficiency and V is the traveling speed. When α, μ and R are assumed to be constant, Eq. (3) [20] can be derived as:

$$Q \propto \frac{PN}{V} = P \cdot a \propto F \cdot a \quad (3)$$

where a is the slope of the traveling speed versus the rotation speed and F is the tool plunge down force.

According to Eq. (3), if the rotation speed N is kept constant, the heat input Q increases linearly with decreasing the traveling speed V. At the lower traveling speed (250 mm/min), there is more heat input Q, so the temperature of SZ is relatively higher. Therefore, the $Al_{11}RE_3$ phase in SZ will grow up in the welding process due to more heat generated, thus the average diameter of the $Al_{11}RE_3$ phase is bigger. Nevertheless, at the higher traveling speed (750 mm/min), because of the less heat input Q, there is no enough heat for the $Al_{11}RE_3$ phase to grow up. This explains that the average diameter of the $Al_{11}RE_3$ phase in SZ decreases with increasing the traveling speed, as shown in Fig. 8.

Similarly, in the same welding condition, the top and middle regions of SZ contain more heat input Q, which also results in the bigger size of $Al_{11}RE_3$ phase, as shown in Fig. 6. In contrast, at the bottom region of SZ there is lest heat input, for which less heat was supplied for the $Al_{11}RE_3$ phase to grow up. This is why the smallest size of $Al_{11}RE_3$ particles is observed in the bottom region among all the regions of SZ in the same welding condition. In a word, the size of $Al_{11}RE_3$ phase in SZ is mainly depended on the heat input, and it decreases with the heat input.

3.5. Mechanical properties after FSW

The hardness was measured at mid-thickness across SZ at different traveling speeds with the constant rotation speed of 1250 rpm, as shown in Fig. 10. The hardness of SZ is evidently higher than that of BM, indicating that both the microstructure and mechanical properties have been modified after FSW. Furthermore, the average hardness in SZ increases slightly with traveling speed at the constant rotation speed, i.e. with decreasing welding heat input.

The tensile strengths and elongations of specimens machined from SZ and BM welded with 1250 rpm rotation speed and 250 traveling speed are presented in Fig. 11, as an example. The tensile strength of BM is 106.67 MPa, while that of SZ is increased to be 127.24 MPa, with the increment of 19%. At the same time, the elongation of SZ is 5.7%, higher than that of BM, 5.0%. This indicates that the mechanical properties have been improved after FSW, which are caused by the finer and uniform microstructure in SZ.

The fracture surfaces of BM and SZ specimens are shown in Fig. 12. Solidification defects such as porosity exist on the fracture surface of BM, while no defect is observed on that of SZ. Besides, the fracture surface of SZ exhibits small dimples, which are probably resulted from the homogeneous microstructure of fine grains. It can be concluded from the above results that FSW is a very useful modification method for the mechanical property improvement, because it refines and uniforms the microstructure and intermetallic compounds.

4. Conclusions

Thixo-molded AE42 Mg alloy was friction stir welded, and the microstructures and mechanical properties after FSW were investigated. The following conclusions can be drawn.

(1) According to the X-ray radiography, the optimum FSW condition range of AE42 alloy is obtained, which exists between AZ61 and AZ31 alloys. It seems that the optimum FSW condition range widens with decreasing the Al content in the Mg alloys.
(2) There are mainly two kinds of compounds in the thixo-molded AE42 alloy, and FSW has little influence on the grainy $Al_{10}RE_2Mn_7$ compound, but it has great influence on the $Al_{11}RE_3$ phase, which has been changed from lamellar eutectic to small particle after FSW. The average diameter of $Al_{11}RE_3$ phase in SZ decreased with increasing the traveling speed at constant rotation speed, due to the less heat input.
(3) The hardness of SZ is higher than that of BM, and the tensile strength and elongation both have been improved after FSW, because FSW refines and uniforms the microstructure and intermetallic compounds.

References

[1] X. Cao, M. Jahazi, J.P. Immarigeon, W. Wallace, Journal of Materials Processing Technology 171 (2006) 188–204.
[2] N. Afrin, D.L. Chen, X. Cao, M. Jahazi, Scripta Materialia 57 (2007) 1004–1007.
[3] E. Aghion, B. Bronfin, Materials Science Forum 350–351 (2000) 19–28.
[4] K. Nakata, Y.G. Kim, H. Fujii, T. Tsumura, T. Komazaki, Materials Science and Engineering A 437 (2006) 274–280.
[5] A.L. Etter, T. Baudin, N. Fredj, R. Penelle, Materials Science and Engineering A 445–446 (2007) 94–99.
[6] J. William, Arbegast, Scripta Materialia 58 (2008) 372–376.
[7] H. Lombard, D.G. Hattingh, A. Steuwer, M.N. James, Engineering Fracture Mechanics 75 (2008) 341–354.
[8] H.B. Chen, K. Yan, T. Lin, S.B. Chen, C.Y. Jiang, Y. Zhao, Materials Science and Engineering A 433 (2006) 64–69.
[9] R.S. Mishra, Z.Y. Ma, Materials Science and Engineering R 50 (2005) 1–78.
[10] G.M. Xie, Z.Y. Ma, L. Geng, R.S. Chen, Materials Science and Engineering A 471 (2007) 63–68.
[11] L. Commin, M. Dumont, J.-E. Masse, L. Barrallier, Acta Materialia 57 (2009) 326–334.

[12] A.H. Feng, Z.Y. Ma, Scripta Materialia 56 (2007) 397–400.
[13] B.M. Darras, M.K. Khraisheh, F.K. Abu-Farha, M.A. Omar, Journal of Materials Processing Technology 191 (2007) 77–81.
[14] R.P. Dobriyal, B.K. Dhindaw, S. Muthukumaran, S.K. Mukherjee, Materials Science and Engineering A 477 (2008) 243–249.
[15] K. Nakata, Y.G. Kim, M. Ushio, Transactions of JWRI 31–2 (2002) 141–146.
[16] I.P. Moreno, T.K. Nandy, J.W. Jones, J.E. Allison, T.M. Pollock, Scripta Materialia 48 (2003) 1029–1034.
[17] G. Pettersen, H. Westengen, R. Hoier, O. Lohne, Materials Science and Engineering A 207 (1996) 115–120.
[18] Y.G. Kim, H. Fujii, T. Tsumura, T. Komazaki, K. Nakata, Materials Letters 60 (2006) 3830–3837.
[19] Ø. Frigaard, Ø. Grong, O.T. Midling, Metallurgical and Materials Transactions A 32 (2001) 1189–1199.
[20] Y.G. Kim, H. Fujii, T. Tsumura, T. Komazaki, K. Nakata, Materials Science and Engineering A 415 (2006) 250–254.